Electronic Supplementary Material (ESI) for Nanoscale.

Abnormally weak intervalley electron scattering in MoS_2 monolayer: insights from the matching between electron and phonon bands

Shiru Song,[a] Ji-Hui Yang*[a,b] and Xin-Gao Gong[a,b]
[a]Key Laboratory of Computational Physical Sciences (Ministry of Education), Institute of Computational Physics, Fudan University, Shanghai 200433, China
Email: jhyang04@fudan.edu.cn
[b]Shanghai Qi Zhi Institute, Shanghai 200230, China

Detailed calculation methods and band edge valleys and partial charge of the hole in MoS_2 monolayer, and other supporting data.

Fig. S1. Band edge valleys and partial charge of the hole in MoS_2 monolayer.

Fig. S2. The phonon-energy resolved hole scattering rates, matching functions, average electron-phonon coupling strength, and phonon-branch resolved scattering in monolayer MoS_2.

Fig. S3. The phonon-energy resolved electron scattering rates, matching functions, average electron-phonon coupling strength, and phonon-branch resolved scattering in monolayer $MoSe_2$.

Fig. S4. The phonon-energy resolved electron scattering rates, matching functions, average electron-phonon coupling strength, and phonon-branch resolved scattering in monolayer WS_2.

Fig. S5. The phonon-energy resolved electron scattering rates, matching functions, average electron-phonon coupling strength, and phonon-branch resolved scattering in the monolayer black phosphorus.

Fig. S6. The phonon-energy resolved hole scattering rates, matching functions, average electron-phonon coupling strength, and phonon-branch resolved scattering in the monolayer BN.

Fig. S7. The Convergence of calculated carrier mobilities with respect to the Brillouin-zone sampling for the monolayer and bulk MoS_2.

Supplementary Note S1: Computation Methods

We perform first-principles calculations using the Quantum Espresso Package[1, 2] with the norm-conserving pseudopotentials[3] and the Perdew-Burke-Ernzerhof (PBE) exchange-correlation functional.[4] The van der Waals interaction in MoS_2 bulk is considered with the nonlocal functional rVV10.[5] The kinetic energy cutoffs for wave functions and charge density are set to 80 and 320 Ry, respectively. The atomic coordinates for bulk MoS_2 are optimized using a 36 × 36 × 8 k mesh until the force acting on each atom becomes less than 0.0001 Ry/Bohr. The monolayer MoS_2 is described using a vacuum-slab model. The length of the cell in the out-of-plane direction is 20 Å for monolayer MoS_2. The Brillouin zone is sampled using a 36 ×36 Monkhorst-Pack mesh. Calculations of electron-phonon couplings and carrier mobilities are performed using the EPW code.[6, 7] For bulk MoS_2, the electron-phonon matrix elements are initially computed on a 18 × 18 × 4 electronic grid and a 9 × 9 × 2 phonon grid, using density functional perturbation theory (DFPT).[8] Then the electron-phonon matrix elements are subsequently interpolated onto fine grids, a 90 × 90 × 21 electronic grid and a 90 × 90 × 21 phonon grid, using maximally localized Wannier functions.[9, 10] For monolayer, the electron-phonon matrix elements are initially computed on a 18 × 18 electronic grid and a 9 × 9 phonon grid, which are subsequently interpolated onto fine grids, i.e., 300 × 300 electronic grid and a 300 × 300 phonon grid. The convergence with respect to the grid size of k and q meshes for monolayer and bulk MoS_2 has been tested. The result is convergent within 2 cm2/Vs. The carrier concentration for computing the mobilities is set to 10^{16} cm^{-3}, and the temperature is set to 300 K for all systems. The convergence with respect to the grid size of k and q meshes for monolayer and bulk MoS_2 has been tested. The result is converged within 2 cm^2/Vs. We have also calculated the mobilities for MoS_2 monolayer and bulk, using the iterative method.[11] The mobilities are 179.9 cm^2/Vs for the monolayer MoS_2, 97.4(∥) cm2/Vs, 112.5(⊥) cm^2/Vs for the bulk MoS_2. The mobility calculations for MoS_2 monolayer using the nonlocal functional rVV10 are tested. In this case, the mobility is 180.0 cm^2/Vs for the monolayer MoS_2 which is still larger than the one for the bulk obtained using rVV10.

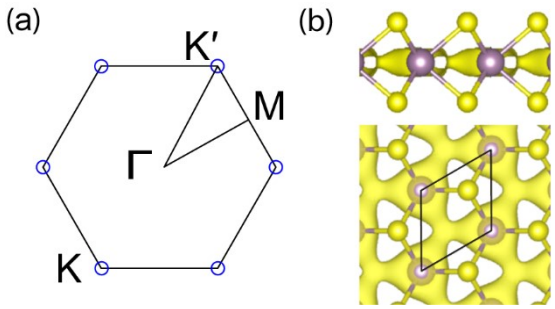

Figure S1. Band edge valleys and partial charge of the hole in MoS_2 monolayer. (a) The VBM valleys in monolayer MoS_2. (b) Top and side view of the VBM partial charge densities.

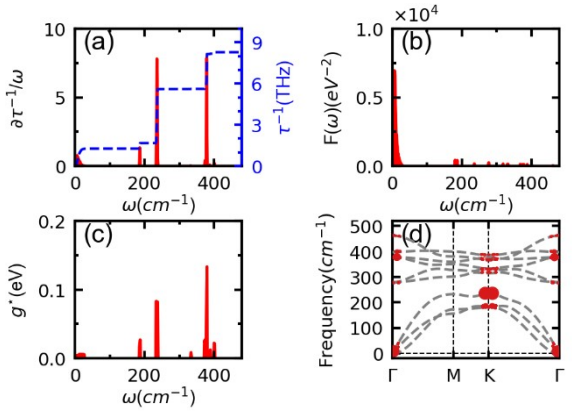

Figure S2. The phonon-energy resolved hole scattering rates, matching functions, average electron-phonon coupling strength, and phonon-branch resolved scattering in monolayer MoS_2. (a) The phonon-spectra-decomposed hole scattering rate. (b) The phonon-energy resolved matching functions between electronic band structure and phonon spectrum. (c) The phonon-energy resolved average electron-phonon coupling strength for monolayer MoS_2. (d) The phonon-branch resolved scattering rates for holes in the MoS_2 monolayer. Note that, the blue lines in (a) indicate the integrated scattering rates and the sizes of the dots in (d) are proportional to the scattering rates assisted by the corresponding phonon modes.

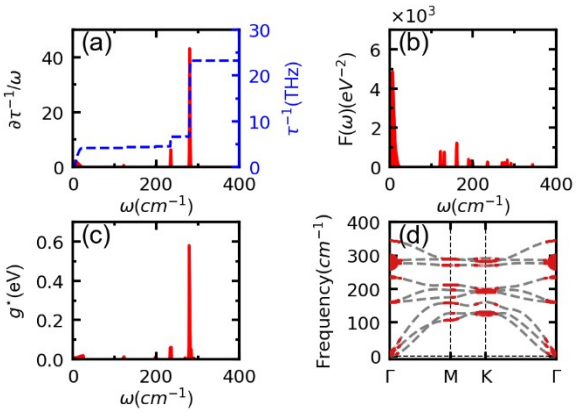

Figure S3. The phonon-energy resolved electron scattering rates, matching functions, average electron-phonon coupling strength, and phonon-branch resolved scattering in monolayer $MoSe_2$. (a) The phonon-spectra-decomposed electron scattering rate. (b) The phonon-energy resolved matching functions between electronic band structure and phonon spectrum. (c) The phonon-energy resolved average electron-phonon coupling strength for monolayer $MoSe_2$. (d) The phonon-branch resolved scattering rates for electrons in the $MoSe_2$ monolayer.

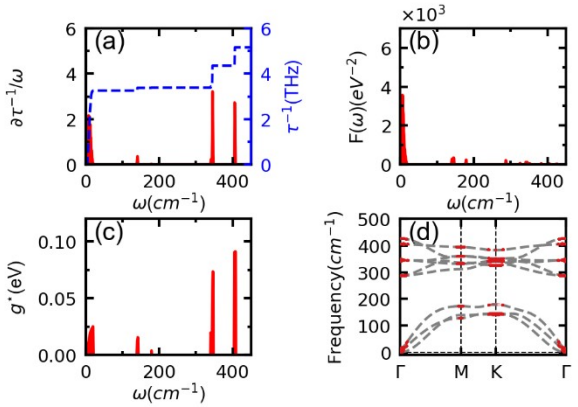

Figure S4. The phonon-energy resolved electron scattering rates, matching functions, average electron-phonon coupling strength, and phonon-branch resolved scattering in monolayer WS_2. (a) The phonon-spectra-decomposed electron scattering rate. (b) The phonon-energy resolved matching functions between electronic band structure and phonon spectrum. (c) The phonon-energy resolved average electron-phonon coupling strength for monolayer WS_2. (d) The phonon-branch resolved scattering rates for electrons in the WS_2 monolayer.

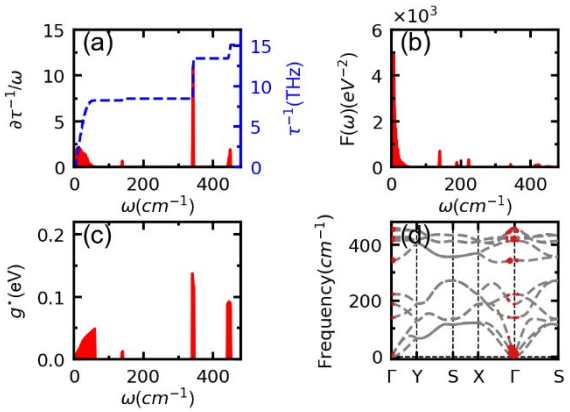

Figure S5. The phonon-energy resolved electron scattering rates, matching functions, average electron-phonon coupling strength, and phonon-branch resolved scattering in the monolayer black phosphorus. (a) The phonon-spectra-decomposed electron scattering rate. (b) The phonon-energy resolved matching functions between electronic band structure and phonon spectrum. (c) The phonon-energy resolved average electron-phonon coupling strength for monolayer black phosphorus. (d) The phonon-branch resolved scattering rates for electrons in the black phosphorus monolayer.

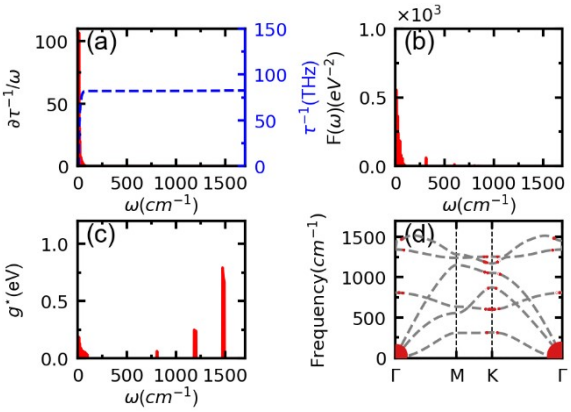

Figure S6. The phonon-energy resolved hole scattering rates, matching functions, average electron-phonon coupling strength, and phonon-branch resolved scattering in the monolayer BN. (a) The phonon-spectra-decomposed hole scattering rate. (b) The phonon-energy resolved matching functions between electronic band structure and phonon spectrum. (c) The phonon-energy resolved average electron-phonon coupling strength for monolayer BN. (d) The phonon-branch resolved scattering rates for holes in the BN monolayer.

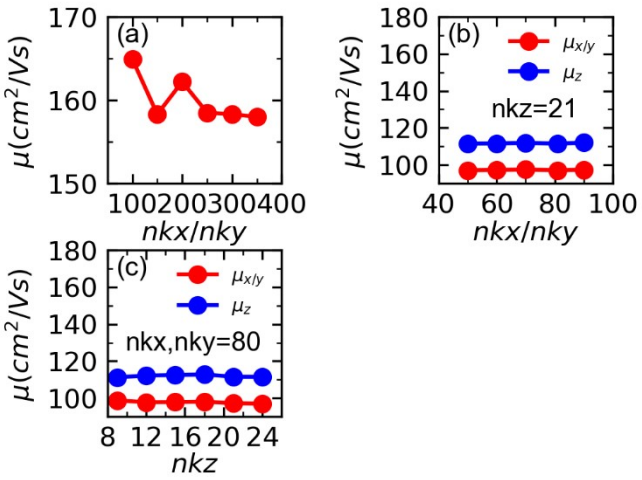

Figure S7. Convergence of calculated carrier mobilities with respect to the Brillouin-zone sampling. (a) Convergence of electron mobility with respect to the number of k/q points along each dimension, for monolayer MoS_2. (b) Convergence of electron mobility along the x/y(z) direction with respect to the number of k/q points nkx/nky along each planar dimension with nkz fixed to 21, for bulk MoS_2. (c) Convergence of electron mobility along the x/y(z) direction with respect to the number of k/q points nkz along the z direction with nkx/nky fixed to 80, for bulk MoS_2.

References

1. P. Giannozzi, S. Baroni, N. Bonini, M. Calandra, R. Car, C. Cavazzoni, D. Ceresoli, G. L. Chiarotti, M. Cococcioni, I. Dabo, A. D. Corso, S. d. Gironcoli, S. Fabris, G. Fratesi, R. Gebauer, U. Gerstmann, C. Gougoussis, A. Kokalj, M. Lazzeri, L. Martin-Samos, N. Marzari, F. Mauri, R. Mazzarello, S. Paolini, A. Pasquarello, L. Paulatto, C. Sbraccia, S. Scandolo, G. Sclauzero, A. P. Seitsonen, A. Smogunov, P. Umari and R. M. Wentzcovitch, *J. Phys.: Condens. Matter*, 2009, **21**, 395502.
2. P. Giannozzi, O. Andreussi, T. Brumme, O. Bunau, M. B. Nardelli, M. Calandra, R. Car, C. Cavazzoni, D. Ceresoli, M. Cococcioni, N. Colonna, I. Carnimeo, A. D. Corso, S. d. Gironcoli, P. Delugas, R. A. DiStasio, A. Ferretti, A. Floris, G. Fratesi, G. Fugallo, R. Gebauer, U. Gerstmann, F. Giustino, T. Gorni, J. Jia, M. Kawamura, H.-Y. Ko, A. Kokalj, E. Küçükbenli, M. Lazzeri, M. Marsili, N. Marzari, F. Mauri, N. L. Nguyen, H.-V. Nguyen, A. Otero-de-la-Roza, L. Paulatto, S. Poncé, D. Rocca, R. Sabatini, B. Santra, M. Schlipf, A. P. Seitsonen, A. Smogunov, I. Timrov, T. Thonhauser, P. Umari, N. Vast, X. Wu and S. Baroni, *J. Phys.: Condens. Matter*, 2017, **29**, 465901.
3. D. R. Hamann, *Phys. Rev. B*, 2013, **88**, 085117.
4. J. P. Perdew, K. Burke and M. Ernzerhof, *Phys. Rev. Lett.*, 1996, **77**, 3865-3868.
5. R. Sabatini, T. Gorni and S. de Gironcoli, *Phys. Rev. B*, 2013, **87**, 041108.
6. S. Poncé, E. R. Margine, C. Verdi and F. Giustino, *Comput. Phys. Commun.*, 2016, **209**, 116-133.
7. F. Giustino, M. L. Cohen and S. G. Louie, *Phys. Rev. B*, 2007, **76**, 165108.
8. F. Giustino, *Rev. Mod. Phys.*, 2017, **89**, 015003.
9. A. A. Mostofi, J. R. Yates, G. Pizzi, Y.-S. Lee, I. Souza, D. Vanderbilt and N. Marzari, *Comput. Phys. Commun.*, 2014, **185**, 2309-2310.
10. G. Pizzi, V. Vitale, R. Arita, S. Blügel, F. Freimuth, G. Géranton, M. Gibertini, D. Gresch, C. Johnson, T. Koretsune, J. Ibañez-Azpiroz, H. Lee, J.-M. Lihm, D. Marchand, A. Marrazzo, Y. Mokrousov, J. I. Mustafa, Y. Nohara, Y. Nomura, L. Paulatto, S. Poncé, T. Ponweiser, J. Qiao, F. Thöle, S. S. Tsirkin, M. l. Wierzbowska, N. Marzari, D. Vanderbilt, I. Souza, A. A. Mostofi and J. R. Yates, *J. Phys.: Condens. Matter*, 2020, **32**, 165902.
11. S. Ponce, W. Li, S. Reichardt and F. Giustino, *Rep. Prog. Phys.*, 2020, **83**, 036501.